

Single electron spin control in semiconductor nanowires

Prabhakar, S., Melnik, R.

**Proceedings of the 8th International Conference on Engineering
Computational Technology (ECT-2012), September 4-7, 2012,
Paper 22, doi:10.4203/ccp.100.22, 2012.**

8th International Conference on Engineering Computational Technology 2012

(ECT 2012)

Civil-Comp Proceedings 100

**Dubrovnik, Croatia
4-7 September 2012**

Volume 1 of 2

Editors:

B. H. V. Topping

ISBN: 978-1-62276-380-1

ISSN: 1759-3433

Printed from e-media with permission by:

Curran Associates, Inc.
57 Morehouse Lane
Red Hook, NY 12571



Some format issues inherent in the e-media version may also appear in this print version.

Copyright© (2012) by Civil-Comp Press
All rights reserved.

Printed by Curran Associates, Inc. (2012)

For permission requests, please contact Civil-Comp Press
at the address below.

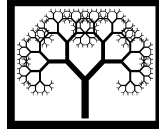
Civil-Comp Press
Dun Eaglais
Station Brae, Kippen
Stirling FK8 3DY
United Kingdom

Phone: +44 (0) 1786 870 166
Fax: +44 (0) 1786 870 167

www.civil-comp.com

Additional copies of this publication are available from:

Curran Associates, Inc.
57 Morehouse Lane
Red Hook, NY 12571 USA
Phone: 845-758-0400
Fax: 845-758-2634
Email: curran@proceedings.com
Web: www.proceedings.com



Single Electron Spin Control in Semiconductor Nanowires

S. Prabhakar¹ and R. Melnik^{1,2}

¹M²NeT Laboratory, Wilfrid Laurier University, Waterloo ON, Canada

²Ikerbasque, Basque Foundation for Science and BCAM, Bilbao, Spain

Abstract

We study the level crossing in the energy spectrum due to Rashba-Dresselhaus spin-orbit coupling in nanowires modulated by longitudinal potential. By implementing both an analytical methodology and a numerical technique based on the finite element method (FEM), we show that the level crossing point can be manipulated with the application of spin-orbit coupling in parabolic nanowires. In particular, the level crossing point can be found at larger values of k in GaAs nanowires compared to those of InAs nanowires due to large values of the Rashba-Dresselhaus spin-orbit coupling in the latter case.

Keywords: semiconductors, quantum wires, spin-orbit coupling, spintronics, perturbation theory, finite element method.

1 Introduction

Electron spin control in low dimensional semiconductor nanostructures such as quantum dots, quantum wells and quantum wires can be defined in the plane of 2 Dimensional Electron Gas (2DEG). Such control is important for spintronic logic devices, optoelectronics, quantum computing and quantum information theory [1, 2, 3, 4, 5, 6, 7]. Low dimensional semiconductors can be experimentally grown by several existing techniques such as lithographic, molecular beam epitaxy (MBE), metal organic chemical vapor deposition (MOCVD) and others. Single electron spins in these nanostructures can be manipulated by several parameters such as the gate controlled electric fields in the lateral direction and externally applied magnetic fields. The Rashba and Dresselhaus spin-orbit couplings provide another efficient way to control the single electron spins in these nanostructures [1, 3, 8]. The Rashba spin-orbit coupling arises due to structural inversion asymmetry in the crystal lattice along the growth direc-

tion [9]. The Dresselhaus spin-orbit coupling arises due to bulk inversion asymmetry in the system [10]. Intersubband-induced spin-orbit coupling interaction in quantum wells with two subbands has been introduced in Refs. [11, 12, 13]. Based on the previous studies, it is known that the induced intersubband spin-orbit coupling in quantum wells is non-zero even in symmetric quantum wells and gives rise to a non-zero spin-Hall conductivity.

In this paper, we develop a theoretical model to find the energy spectrum of the parabolic nanowire formed in the plane of 2DEG modulated by longitudinal potential. By utilizing both analytical expressions based on perturbation theory and numerical methods based on the finite element method, we show that the level crossing point can be manipulated with the application of Rashba-Dresselhaus spin-orbit coupling.

2 Mathematical Model

Our main goal is to find the crossing between the spin states due to the Rashba-Dresselhaus spin-orbit coupling in a III-V semiconductor parabolic nanowire formed in the plane of 2DEG. The schematic diagram of the geometry of the experimental device that we have in mind is similar to Ref. [6]. We consider a 1D parabolic nanowire formed by strip gates (see Fig. 1 of Ref. [6]) in the 2D plane where the truncated Fourier cosines along x-direction provide the longitudinal modulation (for example, see Eq. 2). Therefore, the total Hamiltonian of an infinite quasi-1D parabolic nanowire with uniform Rashba-Dresselhaus spin-orbit coupling in presence of longitudinal modulation potential can be written as [6]:

$$H_{xy} = \frac{\mathbf{p}^2}{2m} + \frac{1}{2}m\omega_0^2 y^2 + \frac{\alpha}{\hbar} (p_y \sigma_x - p_x \sigma_y) + \frac{\beta}{\hbar} (p_x \sigma_x - p_y \sigma_y) + \varepsilon_\nu(k), \quad (1)$$

where $\mathbf{p}^2 = p_x^2 + p_y^2$ is the momentum operator, m is the effective mass, $\alpha = \gamma_R e E$ and $\beta = 0.78 \gamma_D (2m e E / \hbar^2)^{2/3}$ are the strengths of the Rashba and Dresselhaus spin-orbit couplings respectively, γ_R is the Rashba coefficient, γ_D is the Dresselhaus coefficient, and $\omega_0 = \hbar / m \ell_0^2$ is the confinement frequency with ℓ_0 being the oscillator strength. Also, $\sigma_i = (\sigma_x, \sigma_y, \sigma_z)$ are the Pauli spin matrices. The longitudinal modulation potential $\varepsilon_\nu(k)$ is given by

$$\varepsilon_\nu(k) = \frac{1}{2}a_0 + \sum_{j=1}^m [a_j \cos(jk/L) + a_m \cos(mk/L)]. \quad (2)$$

Here we choose $L = 1.2418 \text{ nm}$ and the numerical values of the coefficients $a_j \text{ (meV)}$ are 16.2873, -8.2888, 0.1492, -0.0042, 0.0002, -0.0004, -0.0002, 0.0005 for $(j = 0, 1, 2 \dots 7)$. The momentum along x-direction is a good quantum number i.e., $[p_x, H_{xy}] = 0$ and we consider $\hbar k$ as the eigenvalues of the momentum operator p_x .

To find the energy spectrum of the Hamiltonian (1), it is convenient to rotate the Hamiltonian $\bar{H}_{xy} = e^{-\frac{i\pi\sigma_x}{4}} e^{-\frac{i\theta}{2}} H_{xy} e^{\frac{i\theta}{2}} e^{\frac{i\pi\sigma_x}{4}}$. The new Hamiltonian \bar{H}_{xy} can be written

as

$$\bar{H}_{xy} = \frac{\hbar^2 k^2}{2m} + \left(n + \frac{1}{2}\right) \hbar\omega_0 - k\gamma_{\alpha\beta}\sigma_z + \varepsilon_\nu(k) + \frac{i\gamma_{\alpha\beta}}{\ell_0\sqrt{2}} (a^\dagger - a) (\sigma_x \cos 2\theta - \sigma_z \sin 2\theta), \quad (3)$$

where $\gamma_{\alpha\beta} = \sqrt{\alpha^2 + \beta^2}$, $\cos \theta = \frac{\alpha}{\sqrt{\alpha^2 + \beta^2}}$, $\sin \theta = \frac{\beta}{\sqrt{\alpha^2 + \beta^2}}$. The $\sin 2\theta$ term from

Eq. 3 can be removed by rotating the Hamiltonian $\tilde{H}_{xy} = e^{-\frac{i\gamma_s \hat{y} \sigma_z}{\hbar\omega_0 \ell_0^2}} \bar{H}_{xy} e^{\frac{i\theta}{2}} e^{\frac{i\pi\sigma_x}{4}}$. The new Hamiltonian \tilde{H}_{xy} can be written as

$$\begin{aligned} \tilde{H}_{xy} = & \frac{\hbar^2 k^2}{2m} + \left(n + \frac{1}{2}\right) \hbar\omega_0 + \frac{\gamma_s^2}{2\hbar\omega_0 \ell_0^2} - k\gamma_{\alpha\beta}\sigma_z + \varepsilon_\nu(k) \\ & + \frac{i\gamma_c}{\ell_0\sqrt{8}} \left[\left(a^\dagger - a - \frac{\gamma_s^2}{(\hbar\omega_0 \ell_0)^2} (2a^\dagger + na^\dagger + a - na) \right) \sigma_x + \frac{\sqrt{2}\gamma_s}{\hbar\omega_0 \ell_0} \sigma_y \right], \quad (4) \end{aligned}$$

where $\gamma_s = \gamma_{\alpha\beta} \sin 2\theta$, $\gamma_c = \gamma_{\alpha\beta} \cos 2\theta$ and $\hat{y} = \ell_0/\sqrt{2} (a + a^\dagger)$. It can be seen that the Hamiltonian (4) acts as a shifted parabola. Furthermore, the Hamiltonian (4) can be written as $\tilde{H}_{xy} = H_0 + H_1$ where H_0 is the diagonal part and H_1 is the non-diagonal part. Following Ref. [6], we have

$$H_0 = \frac{\hbar^2 k^2}{2m} + \left(n + \frac{1}{2}\right) \hbar\omega_0 + \frac{\gamma_s^2}{2\hbar\omega_0 \ell_0^2} - k\gamma_{\alpha\beta}\sigma_z + \varepsilon_\nu(k), \quad (5)$$

$$H_1 = \frac{i\gamma_c}{\ell_0\sqrt{8}} \left[\left(a^\dagger - a - \frac{\gamma_s^2}{(\hbar\omega_0 \ell_0)^2} \hat{\gamma}_a \right) \sigma_+ + \left(a^\dagger - a - \frac{\gamma_s^2}{(\hbar\omega_0 \ell_0)^2} \hat{\gamma}_a \right) \sigma_- \right], \quad (6)$$

where $\hat{\gamma}_a = 2a^\dagger + na^\dagger + a - na$ and $\sigma_\pm = \sigma_x \pm \sigma_y$. For a situation where $H_0 \gg H_1$, we use non-diagonal Hamiltonian H_1 as a perturbation. Based on the second order perturbation theory, the energy spectrum of the nanowire can be written as

$$\begin{aligned} \varepsilon_{k,n,+1/2} = & \frac{\hbar^2 k^2}{2m} + \left(n + \frac{1}{2}\right) \hbar\omega_0 + \frac{\gamma_s^2}{2\hbar\omega_0 \ell_0^2} - k\gamma_{\alpha\beta} + \varepsilon_\nu(k) \\ & - \frac{\gamma_c^2 (n+1)}{8\ell_0^2} \left[\frac{\left[1 + \frac{\gamma_s^2}{(\hbar\omega_0 \ell_0)^2} (1-n)\right] \left[1 - \frac{\gamma_s^2}{(\hbar\omega_0 \ell_0)^2} (n+3)\right]}{\hbar\omega_0 + 2k\gamma_{\alpha\beta}} \right] \\ & + \frac{\gamma_c^2 n}{8\ell_0^2} \left[\frac{\left[1 - \frac{\gamma_s^2}{(\hbar\omega_0 \ell_0)^2} (2-n)\right] \left[1 - \frac{\gamma_s^2 n}{(\hbar\omega_0 \ell_0)^2}\right]}{\hbar\omega_0 - 2k\gamma_{\alpha\beta}} \right], \quad (7) \end{aligned}$$

$$\begin{aligned} \varepsilon_{k,n,-1/2} = & \frac{\hbar^2 k^2}{2m} + \left(n + \frac{1}{2}\right) \hbar\omega_0 + \frac{\gamma_s^2}{2\hbar\omega_0 \ell_0^2} + k\gamma_{\alpha\beta} + \varepsilon_\nu(k) \\ & - \frac{\gamma_c^2 (n+1)}{8\ell_0^2} \left[\frac{\left[1 + \frac{\gamma_s^2}{(\hbar\omega_0 \ell_0)^2} (1-n)\right] \left[1 - \frac{\gamma_s^2}{(\hbar\omega_0 \ell_0)^2} (n+3)\right]}{\hbar\omega_0 - 2k\gamma_{\alpha\beta}} \right] \\ & + \frac{\gamma_c^2 n}{8\ell_0^2} \left[\frac{\left[1 - \frac{\gamma_s^2}{(\hbar\omega_0 \ell_0)^2} (2-n)\right] \left[1 - \frac{\gamma_s^2 n}{(\hbar\omega_0 \ell_0)^2}\right]}{\hbar\omega_0 + 2k\gamma_{\alpha\beta}} \right]. \quad (8) \end{aligned}$$

3 Results and Discussions

By utilizing both analytical and numerical techniques, in Fig. 1(a), we study the dispersion relation i.e., energy vs k for several available states in a GaAs nanowire. Here we find that the level crossing takes place approximately at $k \approx 0.4/nm$. This level crossing point is also an accidental degeneracy point that appear in the energy spectrum in Eqs. (7) and (8). It means that this level crossing point can also be theoretically investigated by using the condition $k = \hbar\omega_0/2\gamma_{\alpha\beta}$. In Fig. 1(b), we plot the wave function of electron spin states in the nanowire far away from the level crossing point i.e. at $k = 0.55/nm$. It can be seen that the first excited state wave function (red plot in Fig. 2) corresponds to the state $|k, 1, +1/2\rangle$ which is a clear indication of the level crossing between the spin states $|k, 0, -1/2\rangle$ and $|k, 1, +1/2\rangle$.

In Fig. 2, we plotted energy vs k for several values of the electric fields. It can be seen that the level crossing point can be manipulated to either smaller or larger values of k with the application of Rashba-Dresselhaus spin-orbit coupling.

In Fig. 3, we study the crossing of the energy levels for InAs parabolic nanowires. In this case, the Rashba spin-orbit coupling is much stronger than the Dresselhaus spin-orbit coupling and we find the crossing point at smaller values of k compared to the corresponding values for GaAs material.

4 Conclusions

In conclusion, we have shown that the electron spin states in nanowire modulated by longitudinal potential can be manipulated with the application of Rashba-Dresselhaus spin-orbit coupling. In particular, we have shown that the level crossing point can be moved to either smaller or larger values of k with the application of electric fields that determine the strengths of the Rashba and Dresselhaus spin-orbit couplings.

Acknowledgments

This work has been supported by NSERC and CRC programs (Canada).

References

- [1] S. Prabhakar, and J. E. Raynolds, “Gate control of a quantum dot single-electron spin in realistic confining potentials: Anisotropy effects”, *Phys. Rev. B* **79**, 195307 (2009).
- [2] S. Prabhakar, J. Raynolds, A. Inomata, and R. Melnik, “Manipulation of single electron spin in a GaAs quantum dot through the application of geometric phases: The Feynman disentangling technique”, *Phys. Rev. B* **82**, 195306 (2010).

- [3] S. Prabhakar, J. E. Raynolds, and R. Melnik, “Manipulation of the Landé g factor in InAs quantum dots through the application of anisotropic gate potentials: Exact diagonalization, numerical, and perturbation methods”, *Phys. Rev. B* **84**, 155208 (2011).
- [4] S. Prabhakar, R. V. N. Melnik, and L. L. Bonilla, “The influence of anisotropic gate potentials on the phonon induced spin-flip rate in GaAs quantum dots”, *Applied Physics Letters* **100**, 023108 (2012).
- [5] S. I. Erlingsson, J. C. Egues, and D. Loss, “Energy spectra for quantum wires and two-dimensional electron gases in magnetic fields with Rashba and Dresselhaus spin-orbit interactions”, *Phys. Rev. B* **82**, 155456 (2010).
- [6] G. Thorngilsson, J. C. Egues, D. Loss, and S. I. Erlingsson, “Rashba spin orbit interaction in a quantum wire superlattice”, *Phys. Rev. B* **85**, 045306 (2012).
- [7] Y. A. Nefyodov, A. V. Shchepetilnikov, I. V. Kukushkin, W. Dietsche, and S. Schmult, “Electron g -factor anisotropy in GaAs/Al_{1-x}Ga_xAs quantum wells of different symmetry”, *Phys. Rev. B* **84**, 233302 (2011).
- [8] S. Takahashi, R. S. Deacon, K. Yoshida, A. Oiwa, K. Shibata, K. Hirakawa, Y. Tokura, and S. Tarucha, “Large anisotropy of the spin-Orbit interaction in a single InAs self-assembled quantum dot”, *Phys. Rev. Lett.* **104**, 246801 (2010).
- [9] Y. A. Bychkov, and E. I. Rashba, “Oscillatory effects and the magnetic susceptibility of carriers in inversion layers”, *J. Phys. C: Solid State Phys.* **17**, 6039 (1984).
- [10] G. Dresselhaus, “Spin-orbit coupling effects in zinc blende structures”, *Phys. Rev.* **100**, 580–586 (1955).
- [11] E. Bernardes, J. Schliemann, M. Lee, J. C. Egues, and D. Loss, “Spin-orbit interaction in symmetric wells with two subbands”, *Phys. Rev. Lett.* **99**, 076603 (2007).
- [12] R. S. Calsaverini, E. Bernardes, J. C. Egues, and D. Loss, “Intersubband-induced spin-orbit interaction in quantum wells”, *Phys. Rev. B* **78**, 155313 (2008).
- [13] M. Lee, M. O. Hachiya, E. Bernardes, J. C. Egues, and D. Loss, “Spin hall effect due to intersubband-induced spin-orbit interaction in symmetric quantum wells”, *Phys. Rev. B* **80**, 155314 (2009).

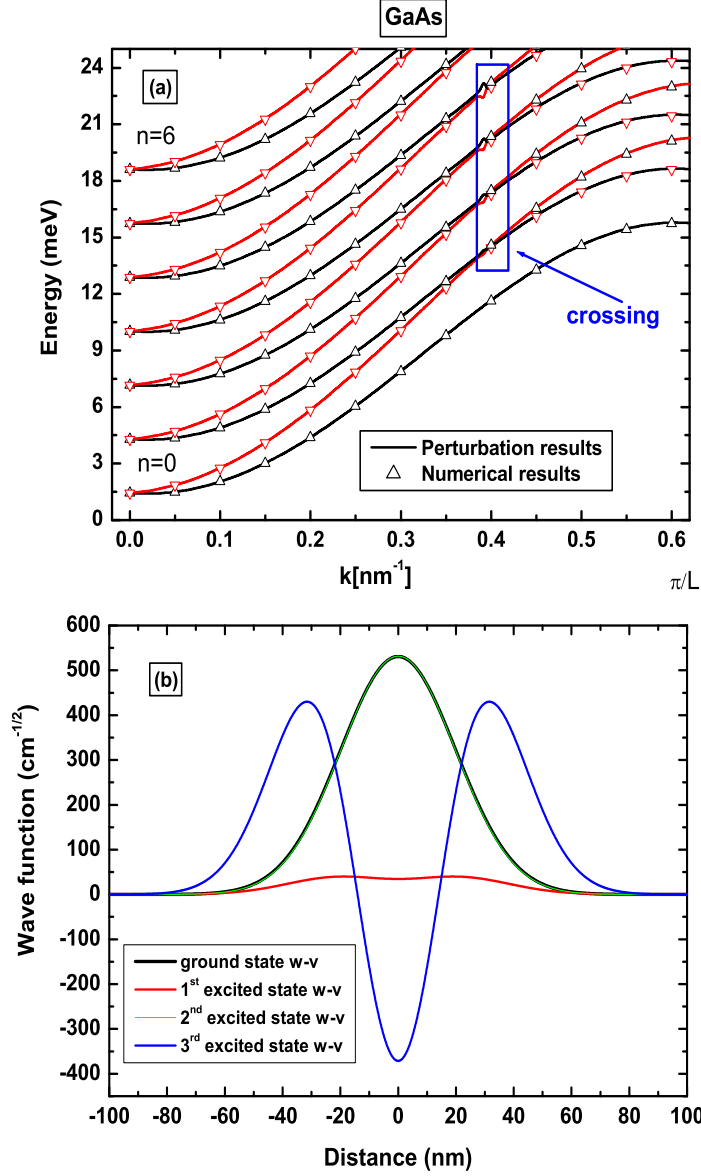


Figure 1: (Color online) (a) Dispersion relation: energy ($\varepsilon - \hbar^2 k^2 / 2m$) vs k . It can be seen that the energy curve corresponding to the state $|k, n, -1/2\rangle$ crosses the energy curve corresponding to the state $|k, n+1, +1/2\rangle$ approximately at $k = 0.4/nm$. (b) Wave function vs distance at $k = 0.55/nm$. The ground state wave function is associated to the state $|k, 0, +1/2\rangle$ (black), the first excited state wave function is associated to the state $|k, 1, +1/2\rangle$ (red), and the second excited state wave function is associated to the state $|k, 0, -1/2\rangle$ (green). Here we chose $E = 3.7 \times 10^5$ V/cm, $\ell_0 = 20$ nm and $\theta = \pi/6$.

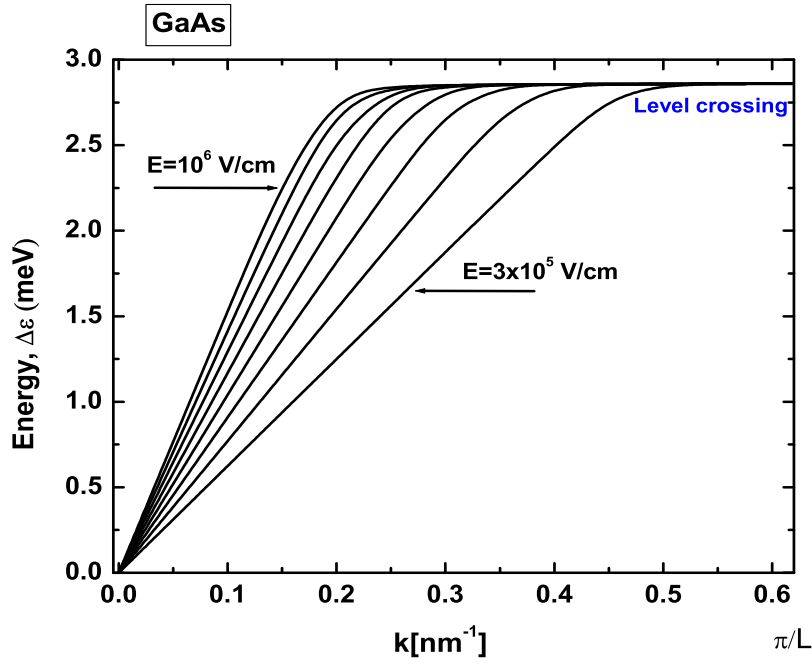


Figure 2: (Color online) Contributions of Rashba-Dresselhaus spin-orbit coupling on electron spins in a nanowire: energy ($\Delta\varepsilon = \varepsilon_{0,-1/2} - \varepsilon_{0,+1/2}$) vs k . The level crossing takes place with the accessible values of k . Here we chose $E = (3, 4 \cdots 10) \times 10^5 \text{ V/cm}$, $\gamma_R = 0.044 \text{ nm}^2$, $\gamma_D = 0.026 \text{ eV nm}^3$, $\ell_0 = 20 \text{ nm}$ and $\theta = \pi/6$.

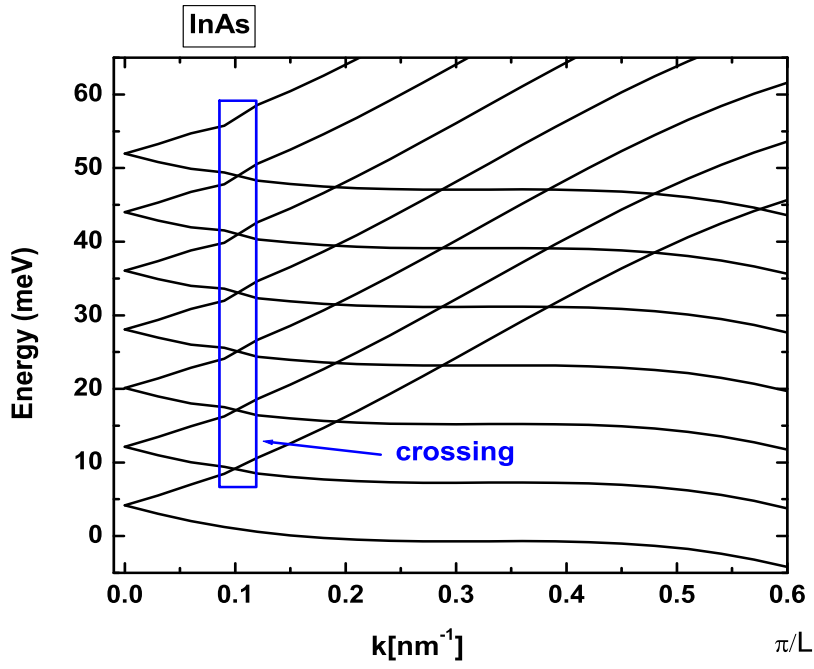


Figure 3: (Color online) Same as Fig. 1(a) but for an InAs nanowire. The level crossing takes place at smaller values of k due to large spin-orbit coupling. Here we chose $\gamma_R = 0.11 \text{ nm}^2$, $\gamma_D = 0.013 \text{ eV nm}^3$.

Contents

Preface

High Performance Computing for Engineering

Special session organised by P. Iványi

1	Future High Performance Computing Strategies M.M. Resch	1
2	Addressing the Problem of Data Mobility for Data-Intensive Science W.E. Johnston, E. Dart and B. Tierney	13
3	On the Design of a Parallel, Distributed Multi-Physics Integration Tool B. Patzák, D. Rypl and J. Kruis	34
4	Load Balancing for Mesh Based Multi-Physics Simulations in the Arcane Framework C. Chevalier, G. Grospellier, F. Ledoux and J.C. Weill	47
5	A Parallelization Algorithm for Non-Smooth Multibody Dynamics J. Clauberg and H. Ulbrich	63
6	Application of GPU-Based Computing to Large Scale Finite Element Analysis of Three-Dimensional Structures A. Akbariyeh, T.J. Carrigan, B.H. Dennis, W.S. Chan, B.P. Wang and K.L. Lawrence	77
7	Adjoining Hybrid Parallel Code M. Schanen, M. Foerster, J. Lotz, K. Leppkes and U. Naumann	89
8	Memory-Region Thread Level Speculative Execution D. Rubio Bonilla and L. Schubert	107
9	A Parallel Meshless Numerical Approach for the Solution of Transport Phenomena G. Kosec and R. Trobec	125
10	The Analysis of Particle Flow using the Parallelised Smoothed Particle Hydrodynamics Method M. Lee, M. Tak and T. Park	137
11	The Analysis of Porous Media using the Mixed Finite Element Method and the FETI Method K. Lee, M. Tak and T. Park	150
12	Platform as a Service Computing Environment for Earthquake Engineering M. Dolenc and R. Klinc	161

Coupled and Multi-Scale Methods

Special session organised by J. Kruis

13	Modelling of Moisture Transfer in Soils T. Krejci and T. Koudelka	168
14	Adaptive Modification of the Künzle Model for Coupled Heat and Moisture Transfer J. Kruis, J. Maděra and P. Šolín	188
15	Processor Farming in Homogenization of Coupled Heat and Moisture Transfer J. Kruis, T. Krejčí, J. Sýkora and M. Šejnoha	204
16	The Local Discontinuous Galerkin Method for Coupled Unsaturated Flow and Chemical Transport in Porous Media A. Ghavam-Nasiri and A. El-Zein	217
17	A Coupled Chemical and Mass Transport Model for Concrete Durability M.M. Jensen, B. Johannesson and M. Geiker	230
18	A Finite Strain Thermo-Chemo-Mechanical Coupled Model for Filled Rubber T.A. Nguyen Van, S. Lejeunes, D. Eyheramendy and A. Boukamel	248
19	The Three Dimensional Extended Bridging Domain Method for Brittle Fracture H. Talebi, M. Silani and T. Rabczuk	268
20	Experimental and Numerical Analysis of the Long Term Behaviour of Glued Laminated Timber R. Pecenko, T. Hozjan, T. Pazlar and G. Turk	287
21	Application of Micromechanics in Engineering Practice M. Šejnoha, V. Šmilauer, J. Němeček and L. Kopecký	301
22	Single Electron Spin Control in Semiconductor Nanowires S. Prabhakar and R. Melnik	318

Analytical and Experimental Performance of Hybrid, Composite, Concrete Structural Systems and Tower Cranes

Special session organised by H.C. Kim, W.K. Hong and Y.S. Shin

23	Progressive Collapse Resisting Capacity of Moment Frames with Infill Steel Panels M.H. Lee, H. Lee and J.K. Kim	326
24	The Design of Special Truss Moment Frames Against Progressive Collapse H.K. Kang, J.Y. Park and J.K. Kim	334
25	The Effect of Cross Sectional Area on the Fire Performance of High Strength Concrete Columns H.S. Kim, Y.H. Kim and Y.S. Shin	341
26	Management Processes for Tower Crane Selection and Support Design C.Y. Lim, K.Y. Son, Y.J. Na and S.K. Kim	352
27	The Effect of Fibre Reinforced Polymer Sizes on Debonding when Retrofitting Reinforced Concrete Beams Y.H. Kim, Y.S. Shin and H.S. Kim	362